JACS
JOURNAL OF THE AMERICAN CHEMICAL SOCIETY

Article

pubs.acs.org/JACS

Fluorescent Probe HKSOX-1 for Imaging and Detection of Endogenous Superoxide in Live Cells and In Vivo

Jun Jacob Hu,[†,∥] Nai-Kei Wong,[†,∥] Sen Ye,[†] Xingmiao Chen,[‡] Ming-Yang Lu,[†] Angela Qian Zhao,[†] Yuhan Guo,[§] Alvin Chun-Hang Ma,[§] Anskar Yu-Hung Leung,[§] Jiangang Shen,[‡] and Dan Yang*[,†]

[†]Morningside Laboratory for Chemical Biology and Department of Chemistry, [‡]School of Chinese Medicine, and [§]Department of Medicine, LKS Faculty of Medicine, The University of Hong Kong, Pokfulam Road, Hong Kong, P. R. China

Ⓦ *Web-Enhanced Feature* Ⓢ *Supporting Information*

ABSTRACT: Superoxide anion radical ($O_2^{\bullet-}$) is undoubtedly the most important primary reactive oxygen species (ROS) found in cells, whose formation and fate are intertwined with diverse physiological and pathological processes. Here we report a highly sensitive and selective $O_2^{\bullet-}$ detecting strategy involving $O_2^{\bullet-}$ cleavage of an aryl trifluoromethanesulfonate group to yield a free phenol. We have synthesized three new $O_2^{\bullet-}$ fluorescent probes (**HKSOX-1**, **HKSOX-1r** for cellular retention, and **HKSOX-1m** for mitochondria-targeting) which exhibit excellent selectivity and sensitivity toward $O_2^{\bullet-}$ over a broad range of pH, strong oxidants, and abundant reductants found in cells. In confocal imaging, flow cytometry, and 96-well microplate assay, **HKSOX-1r** has been robustly applied to detect $O_2^{\bullet-}$ in multiple cellular models, such as inflammation and mitochondrial stress. Additionally, our probes can be efficiently applied to visualize $O_2^{\bullet-}$ in intact live zebrafish embryos. These probes open up exciting opportunities for unmasking the roles of $O_2^{\bullet-}$ in health and disease.

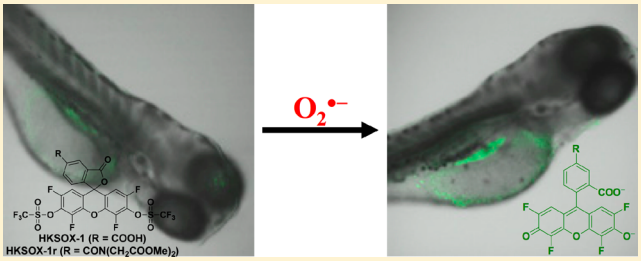

INTRODUCTION

Superoxide anion radical ($O_2^{\bullet-}$) has long been recognized as a vital cellular signaling molecule involved in a plethora of physiological and pathological processes including innate immunity and metabolic homeostasis.[1−3] Aberrant production of $O_2^{\bullet-}$ can lead to oxidative damage of biomolecules such as iron−sulfur (Fe−S) proteins[4−6] and cysteine thiols,[7] or directly induce cell death in bacterial and mammalian cells alike.[8] Its secondary products, such as hydrogen peroxide (H_2O_2), hydroxyl radical ($^{\bullet}OH$), peroxynitrite ($ONOO^-$), and hypochlorous acid (HOCl), are also involved in signal transduction and diverse pathological conditions, including pulmonary arterial hypertension,[9] cardiomyopathy,[9] atherosclerosis,[10] ischemia-reperfusion injury,[9] diabetes mellitus,[9] rheumatoid arthritis,[9] autism,[11] Alzheimer's disease,[12] Parkinson's disease,[9] amyotrophic lateral sclerosis,[9] and cancer.[13,14] Accumulating evidence suggests that imbalances in ROS production frequently concur with mitochondrial dysfunction and disease development.[9] Nevertheless, due to great differences in chemical properties of various ROS (such as half-life, reactivity, and compartmental distribution) and biochemical complexity of cellular milieu (such as pH, antioxidants, and detoxification systems), specific detection of single ROS in live cells and tissues should be of tremendous help to clarify controversial effects of a specific ROS in biological phenomena.[2,8,14−17]

In comparison to indirect measurements, development of selective and sensitive fluorescent probes for $O_2^{\bullet-}$ detection enables direct approaches to quantitate, characterize and predict ROS events. However, lack of reliable fluorescent probes for accurate $O_2^{\bullet-}$ detection in biological systems has hampered mechanistic research on ROS signaling, mitochondria biology, and related diseases.[18,19] Among all available tools for $O_2^{\bullet-}$ detection, hydroethidine (HE) and its mitochondria-targeting analogue MitoSOX have been extensively used,[20] despite that they suffer from limitations of nonspecific DNA-staining and autoxidation,[21] resulting in poor selectivity and sensitivity, as well as inappropriate cellular localization.[21,22] A major challenge in achieving reliable $O_2^{\bullet-}$ sensing is to develop small-molecule fluorescent probes that selectively detect $O_2^{\bullet-}$ in the presence of other reactive species in cells, in particular, highly reactive oxygen species (hROS; up to μM concentration) and ubiquitous thiols (in mM concentrations).[23,24] Previously, several $O_2^{\bullet-}$ fluorescent probes employing nonredox strategies were reported to afford respectable selectivity over other ROS, though they still suffered clear interference from cellular reductants such as cysteine, glutathione (GSH; in mM concentrations) and Fe^{2+} (in μM concentrations), which renders those probes unsuitable for cell imaging.[25−28]

Here we report the development of three novel $O_2^{\bullet-}$ fluorescent probes (**HKSOX-1**, **HKSOX-1r**, and **HKSOX-1m**) via a nonredox strategy for ultrasensitive and selective detection of $O_2^{\bullet-}$ in live cells without the interference of cellular reductants and pH.

Received: February 20, 2015
Published: May 19, 2015

DOI: 10.1021/jacs.5b01881
J. Am. Chem. Soc. 2015, 137, 6837−6843

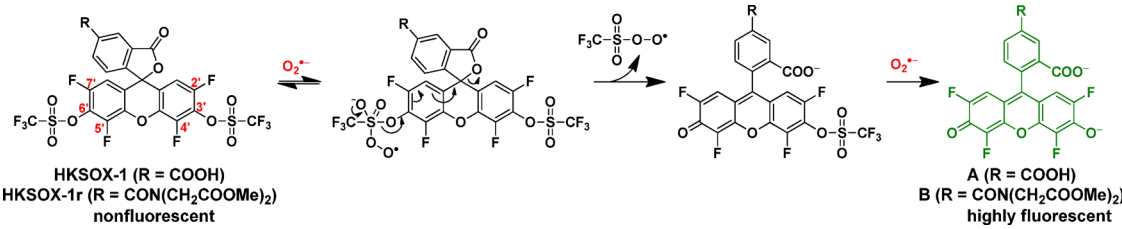

Figure 1. Design of new fluorescent probes **HKSOX-1** and **HKSOX-1r** for $O_2^{\bullet-}$ detection.

RESULTS AND DISCUSSION

Design and Synthesis of Fluorescent Probes. Inspired by previous works on nonredox strategy for $O_2^{\bullet-}$ sensing, we designed an aromatic framework with phenol OH group protected as trifluoromethanesulfonate group. On the one hand, the triflate group is unreactive toward abundant cellular reductants at neutral pH. On the other hand, the trifluoromethyl group is a small but strong electron-withdrawing group that can activate the sulfonate ester toward nucleophilic attack by $O_2^{\bullet-}$, yielding a free phenol. This nonredox reaction can be exploited to tune the fluorescence properties of xanthenes, such as fluorescein, rhodol, and naphthofluorescein. In particular, we envisioned that installation of triflate ester groups at the 3′ and 6′ positions of xanthenes would quench their fluorescence due to lactone ring formation, while the free xanthenes can be released upon treatment with $O_2^{\bullet-}$, leading to turn-on fluorescence (Figure 1).

We selected a special fluorescein, 5-carboxy-2′,4′,5′,7′-tetrafluorofluorescein (ε = 78 100 cm^{-1} M^{-1}, Φ_{fl} = 0.59),[29] as the fluorophore template because of its lower pK_a (3.7) and much greater photostability compared with fluorescein (pK_a = 6.5). The lower pK_a (3.7) ensures application of the probe even under quite acidic conditions (pH = 4.0) in cells, whereas fluorescein cannot turn on efficiently under low pH. By one-step triflation, we prepared **HKSOX-1**, which was then coupled with dimethyl iminodiacetate to yield **HKSOX-1r** for better cellular uptake and retention.[30] To prepare mitochondria-targeting probe **HKSOX-1m**, tetrafluorofluorescein derivative **1** was conjugated with a positively charged triphenylphosphonium moiety, followed by MOM deprotection with acid and triflation (Scheme 1).

Scheme 1[a]

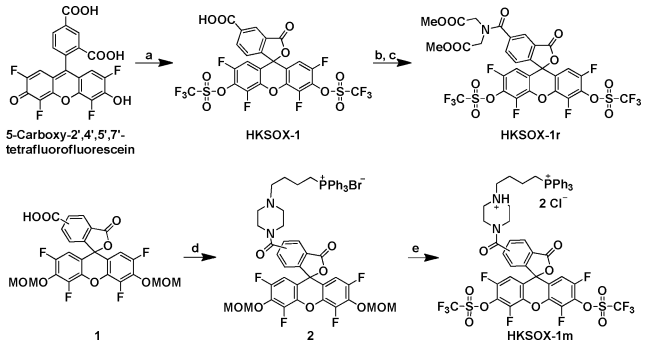

[a]Synthesis of **HKSOX-1**, **HKSOX-1r**, and **HKSOX-1m**. Reagents and conditions: (a) Tf_2O, pyridine, DCM, −78 to 25 °C, 20 min, 41%; (b) DMF, $SOCl_2$, 75 °C, 1 h, 100%; (c) dimethyl iminodiacetate, K_2CO_3, DCM, 25 °C, 12 h, 72%. (d) **3**, EEDQ, DCM, rt, 12 h, 81%; (e) 4 M HCl in 1,4-dioxane, rt, 30 min; Tf_2O, DCM, pyridine, −78 °C to rt, 20 min; Amberlite IRA-400 (Cl), 10 min, 78%.

Reactivity and Selectivity of HKSOX-1 for Superoxide. The reaction of **HKSOX-1** (10 μM) with $O_2^{\bullet-}$ (10 equiv, 100 μM) generated by enzymatic reaction of xanthine (X; 300 μM) and xanthine oxidase (XO; 0.01 U/mL)[25,27] in potassium phosphate buffer (0.1 M, pH 7.4, 0.1% DMF) at 25 °C yielded a dramatic time-dependent fluorescence increase, which was completed within 10 min (Figures S1 and S2). This suggests a very rapid reaction between the probe and $O_2^{\bullet-}$, with a rate constant of ca. 2.0 × 10^5 M^{-1} s^{-1} (see the Supporting Information for details), which is comparable to that of HE (2.6 × 10^5 M^{-1} s^{-1}).[31] Furthermore, the fluorescence intensity remained unchanged within 60 min, indicating high chemostability of the fluorescent product (Figure S2). The identity of the product was proven to be 5-carboxy-2′,4′,5′,7′-tetrafluorofluorescein, which was also obtained in 92% yield when **HKSOX-1** was treated with KO_2 at 25 °C for 10 min in neutral potassium phosphate buffer (Supporting Information). The excellent stability of **HKSOX-1** toward pH changes in the range of 2.2−8.8 further confirms its reliability for cellular $O_2^{\bullet-}$ detection (Figure S3).

Next, different concentrations of $O_2^{\bullet-}$ (0−100 μM) generated by X/XO were added to the testing solutions containing 10 μM **HKSOX-1** (Figure 2a). The fluorescence intensity of the resulting solution was found to increase linearly with the concentrations of $O_2^{\bullet-}$ (0−13 μM; Figure 2b), and the detection limit was estimated to be as low as 23 nM (signal/noise: S/N = 3). As shown in Figure 2a, the fluorescence intensity became saturated when 2 equiv of $O_2^{\bullet-}$ was added. This result is in good agreement with the reaction stoichiometry in our proposed mechanism (Figure 1).[32]

The specificity of **HKSOX-1** was examined by measuring its fluorescence response after exposure to various analytes in potassium phosphate buffer (0.1 M, pH 7.4). As shown in Figure 2c, a >650-fold enhancement in fluorescence intensity was observed toward 4 equiv of $O_2^{\bullet-}$, while 10 equiv (100 μM) of other strong oxidants (H_2O_2, $^{\bullet}NO$, $^1O_2$, $ROO^{\bullet}$, TBHP, $^{\bullet}OH$, $ONOO^-$, and HOCl), reductants (Fe^{2+}, ascorbic acid, and 1,4-hydroquinone) and esterase (0.4 U/mL) could only give negligible fluorescence increase. Strikingly, the fluorescence response of **HKSOX-1** to high concentration of glutathione (GSH; 5 mM, 500 equiv) was only slightly higher than that of other analytes. Thus, the probe exhibited at least 66−100 fold selectivity toward $O_2^{\bullet-}$ over other analytes (Figure 2c and Table S1). In addition, when incubated with $O_2^{\bullet-}$ scavenger TEMPOL (40 μM), $O_2^{\bullet-}$ decomposition catalyst FeTMPyP (40 μM) or superoxide dismutase (SOD; 40 U/mL), the fluorescence intensity could be reduced to basal level. These results demonstrate the excellent selectivity of **HKSOX-1** for $O_2^{\bullet-}$ over other much stronger oxidants, reductants, or even abundant GSH, thus suggesting its potential utility as a molecular probe for detecting $O_2^{\bullet-}$ in cells.

DOI: 10.1021/jacs.5b01881
J. Am. Chem. Soc. 2015, 137, 6837−6843

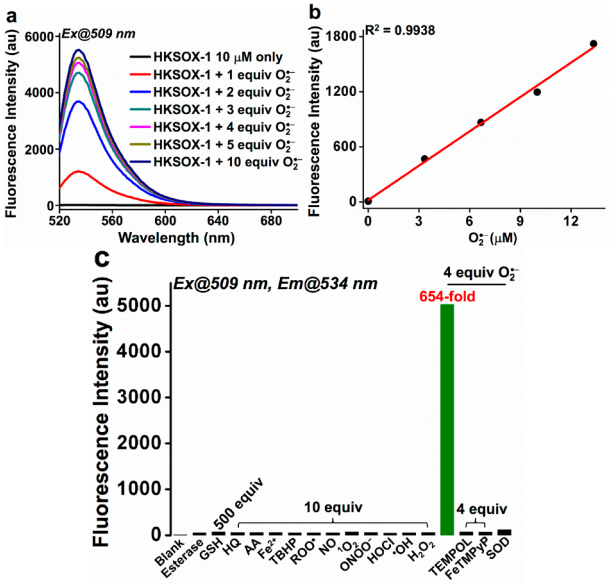

Figure 2. **HKSOX-1** reacts with $O_2^{\bullet-}$ to give a turn-on fluorescence response. Fluorescence spectra of **HKSOX-1** (10 μM) in potassium phosphate buffer (0.1 M, pH 7.4, 0.1% DMF) at 25 °C for 30 min. (a) Incubation with different concentrations of $O_2^{\bullet-}$ (10, 20, 30, 40, 50, and 100 μM) by enzymatic reaction of xanthine (X) and xanthine oxidase (XO) at 25 °C for 30 min. (b) Linear relationship between fluorescence intensity of **HKSOX-1** (10 μM) and concentration of $O_2^{\bullet-}$ (0–13 μM). (c) Incubation with various ROS/RNS and other biological compounds at 25 °C for 30 min. The $O_2^{\bullet-}$ scavengers (TEMPOL and SOD) and $O_2^{\bullet-}$ decomposition catalyst (FeTMPyP) were added to remove $O_2^{\bullet-}$ generated by X/XO. The fluorescence intensity was measured at 534 nm by excitation at 509 nm.

Evaluation of HKSOX-1r/1m for Endogenous Superoxide Detection in Live Cells and In Vivo. To establish applicability of **HKSOX-1r** in cellular studies, we first employed mitochondrial stress as a metabolic model. Mitochondria play crucial roles in a plethora of cellular processes such as energy homeostasis, lipid metabolism, innate immunity, aging and cell death.[2,33,34] Inhibition of mitochondrial electron transfer chain is a well-defined method to induce mitochondrial $O_2^{\bullet-}$ production.[35] By using four mitochondrial respiratory inhibitors,[36] rotenone (complex I inhibitor; 5 μM), FCCP (complex II inhibitor; 5 μM), malonic acid (endogenous complex II inhibitor; 500 μM), and antimycin A (complex III inhibitor; 5 μM), we tested the performance of **HKSOX-1r** in confocal imaging in different cell types: HCT116 (human colon cancer cells), BV-2 (mouse microglia), and RAW264.7 (mouse macrophages). Within 30 min of inhibitor challenge, a robust fluorescence response was reported in all three cell types (Figure 3a and b). Interestingly, an order of efficacy was revealed: antimycin A > FCCP > rotenone > malonic acid. Two-photon confocal imaging indicated that maximal superoxide production induced by antimycin A was only found in the cytoplasm (Figure S4), suggesting that the primary source of superoxide was cytoplasmically localized. By addition of a gradient of mito-TEMPO (a mitochondria-targeting superoxide scavenger), superoxide signal was dose-dependently ablated (Figure S5). Remarkable sensitivity of **HKSOX-1r** was further demonstrated in antimycin A dose-dependency imaging, in which as little as 50 nM antimycin A could yield a detectable fluorescence change (Figure 3c). Kinetically, $O_2^{\bullet-}$ formation induced by antimycin A (5 μM) was shown to be unexpectedly rapid, reaching a plateau in about 10 min in RAW264.7 cells (Figure 3d).

Encouraged by its excellent sensitivity in cell imaging, we next attempted the use of **HKSOX-1r** in 96-well microplate assay as a quantitative platform. **HKSOX-1r** showed dose-dependent fluorescence response (concentration range: 0.05–10 μM) toward FCCP, antimycin A, and the complex V inhibitor oligomycin A in RAW264.7 cells (Figure 4), in agreement with confocal imaging results (Figure S6). To our best knowledge, this is the first example of small-molecule probes for sensitive detection of endogenous $O_2^{\bullet-}$ in quantitative microplate assays.

As a definitive quantitative application for detecting $O_2^{\bullet-}$ in live cells, flow cytometry (FACS) analysis with **HKSOX-1r** was explored. Again, **HKSOX-1r** showed outstanding sensitivity in fluorescence response toward antimycin A challenge (50 nM to 10 μM) in RAW264.7 cells (Figure S7a). $O_2^{\bullet-}$ signal induced by antimycin A (1 μM) was efficiently reduced by the general antioxidant NAC (*N*-acetylcysteine; 10 mM) (Figure 5). In trials with PMA (phorbol 12-myristate 13-acetate) as an oxidative burst stimulant, similarly robust response was elicited (Figure S7b). Overall, our FACS results suggest that **HKSOX-1r** has strong potential applicability in this quantitative platform.

Based on its parent molecule **HKSOX-1**, **HKSOX-1m**, a mitochondria-targeting probe, was synthesized for visualizing mitochondrial $O_2^{\bullet-}$ dynamics. In confocal imaging, **HKSOX-1m** (10 μM) sensitively captured signals for basal and antimycin A (1 μM)-stimulated mitochondrial $O_2^{\bullet-}$ in differentiated human THP-1 cells (Figure S8), at very low laser power output (1% intensity at Ex 514 nm on Zeiss LSM 510 Meta). By using this setting, rapid time-lapse monitoring of mitochondrial $O_2^{\bullet-}$ in both resting and antimycin A-challenged THP-1 cells can be easily performed without any signs of photobleaching (Videos 1 and 2 of time-series imaging are available).

Having established **HKSOX-1r** as a facile cell imaging tool, we proceeded to examine its practical utility in an oxidative burst model, which mimics aspects of inflammation. Oxidative burst or rapid production of ROS is characteristic of mammalian phagocytes as a first-line defense in innate immunity against a broad range of microbial pathogens.[37−39] In particular, phagocyte $O_2^{\bullet-}$ production by enzymatic systems such as NADPH oxidases (NOX) is a critical event in the complex cascades leading to cellular redox reprogramming, production of microbicidal secondary ROS, and eventual pathogen clearance.[37] However, the dynamics of $O_2^{\bullet-}$ production has not been fully characterized.

To address this, we set out to verify the selectivity of **HKSOX-1r** in LPS/IFN-γ stimulated mouse macrophages, in which NOX is a well-documented $O_2^{\bullet-}$ source during inflammation.[34] RAW264.7 cells were challenged overnight (14 h) with bacterial endotoxin lipopolysaccharide (LPS, from *Salmonella typhimurium*; 500 ng/mL) and proinflammatory cytokine interferon-γ (IFN-γ, from mouse; 50 ng/mL) as described previously,[40] in the presence or absence of various NOX inhibitors and $O_2^{\bullet-}$ scavengers (Figure 6a). LPS/IFN-γ treatment induced a maximal level of $O_2^{\bullet-}$ production as reflected by the fluorescence response of **HKSOX-1r**, which was potently inhibited with the addition of the nonspecific NOX inhibitor DPI (dibenziodolium chloride; 50 nM) and specific NOX inhibitor gp91ds-tat (2.5 μM), or $O_2^{\bullet-}$ scavenger FeTMPyP (50 μM). Hence, it is confirmed that **HKSOX-1r**

DOI: 10.1021/jacs.5b01881
J. Am. Chem. Soc. 2015, 137, 6837−6843

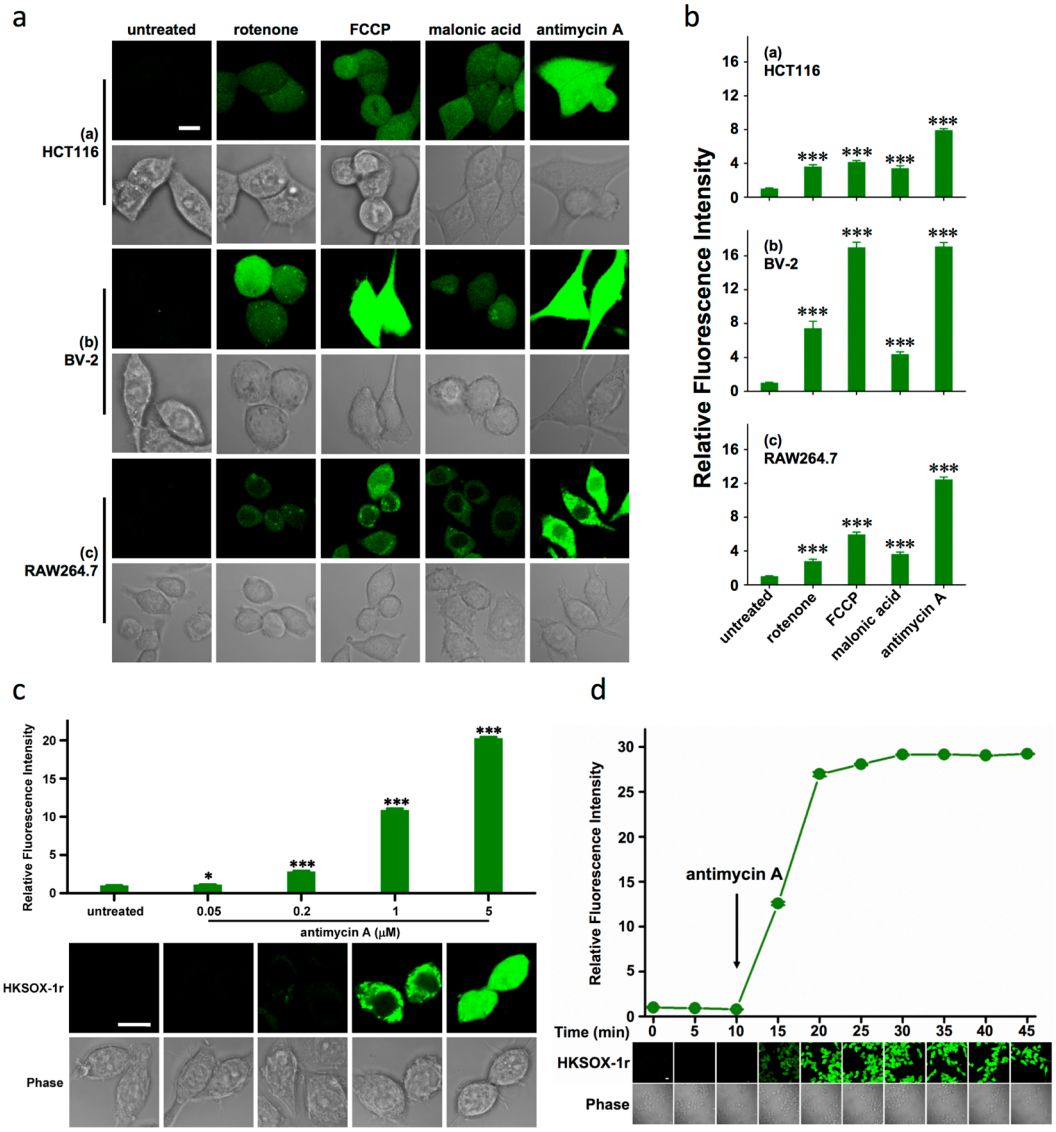

Figure 3. HKSOX-1r detects mitochondrial respiratory inhibitor-induced $O_2^{\bullet-}$ formation in a highly sensitive and rapid manner. (a) Representative images of HCT116 human colon cancer cells, BV-2 mouse microglia or RAW264.7 mouse macrophages coincubated with **HKSOX-1r** (2 μM) and mitochondrial respiratory inhibitor rotenone (5 μM), FCCP (5 μM), malonic acid (500 μM), or antimycin A (5 μM) for 30 min, before confocal imaging. Scale bar = 10 μm. (b) Quantified relative fluorescence intensities of cells as used in (a). Data are mean ± SEM; n = 13−22 cells; ***p < 0.001 versus untreated cells. (c) Representative images of RAW264.7 cells coincubated with **HKSOX-1r** (2 μM) and a dose gradient of antimycin A (50 nM to 5 μM) for 30 min, before confocal imaging at high magnification (315×) (below). Relative mean fluorescence levels of cells in the same groups imaged at lower magnification (63×) were quantified (above). Data are mean ± SEM, n = 50−100 cells; *p < 0.05; ***p < 0.001 versus untreated cells. Scale bar = 10 μm. (d) RAW264.7 cells were first preloaded with **HKSOX-1r** (2 μM) for 30 min before confocal imaging. Basal $O_2^{\bullet-}$ levels were monitored for 10 min, followed by antimycin A (5 μM) challenge (arrow), and further observation (35 min) for fluorescence changes at 5 min intervals, at adjacent locations of the same dish of cells. Data are mean ± SEM; n = 46−73 cells. Scale bar = 10 μm. Results are representative of three independent experiments.

can be used to selectively detect endogenous $O_2^{\bullet-}$ produced enzymatically during inflammation. As oxidative burst has been described in the literature to occur quite rapidly in phagocytes such as neutrophils and macrophages in response to certain PAMPs (pathogen-associated molecular patterns),[35] we assessed how RAW264.7 cells respond to a range of established oxidative burst stimulants including PMA, *f*MLP (*N*-formyl-Met-Leu-Phe), CytoD (cytochalasin D), and zymosan (from *Saccharomyces cerevisiae*).[41−44] Upon 30 min challenge, PMA, a nonspecific PKC (protein kinase C) activator, induced an increase in $O_2^{\bullet-}$ related **HKSOX-1r** response, which can be effectively attenuated by the addition of DPI (50 nM) or a PKC inhibitor (Gö6983, Gö6976 100, or Ro32-0432; 100 nM) (Figure 6b). These results are consistent with literature descriptions that NOX-derived $O_2^{\bullet-}$ production is regulated by PKCs.[44]

Interestingly, the TLR2 (Toll-like receptor 2) ligand zymosan rapidly triggered $O_2^{\bullet-}$ formation which was highly localized (Figure S9). Other immunostimulatory molecules such as *f*MLP, a bacterial oligopeptide that induces phagocyte chemotaxis, and CytoD, a fungal alkaloid with inhibitory activity against phagocytosis, also dose-dependently induced $O_2^{\bullet-}$ production in RAW264.7 cells (Figures S10 and S11), suggesting that **HKSOX-1r** can be used to selectively detect $O_2^{\bullet-}$ in diverse cellular contexts. In addition, the cytotoxicity of **HKSOX-1/1r/1m** were assessed in RAW264.7 or THP-1 cells

DOI: 10.1021/jacs.5b01881
J. Am. Chem. Soc. 2015, 137, 6837−6843

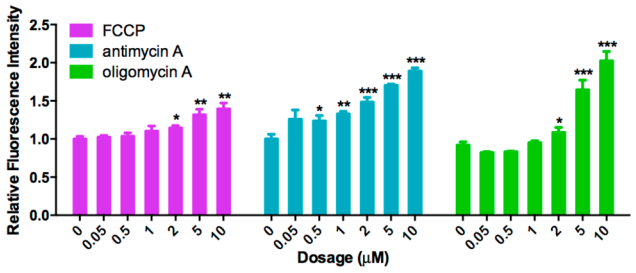

Figure 4. HKSOX-1r sensitively detects $O_2^{\bullet-}$ induced by FCCP, antimycin A and oligomycin A in 96-well microplate fluorometric measurement. RAW264.7 cells were preloaded with **HKSOX-1r** (2 μM in 50 μL HBSS) for 30 min. A dose gradient of FCCP, antimycin A or oligomycin A (dissolved in 50 μL HBSS buffer with 2 μM **HKSOX-1r**) was added to achieve the required drug concentrations (0.05−10 μM) for further incubation for another 30 min, before fluorescence reading. Data are presented, without subtraction of background fluorescence, as mean ± SEM for fluorometric measurement with replicates (n = 4) in at least three independent experiments; *p < 0.05; **p < 0.01; ***p < 0.001 versus untreated cells.

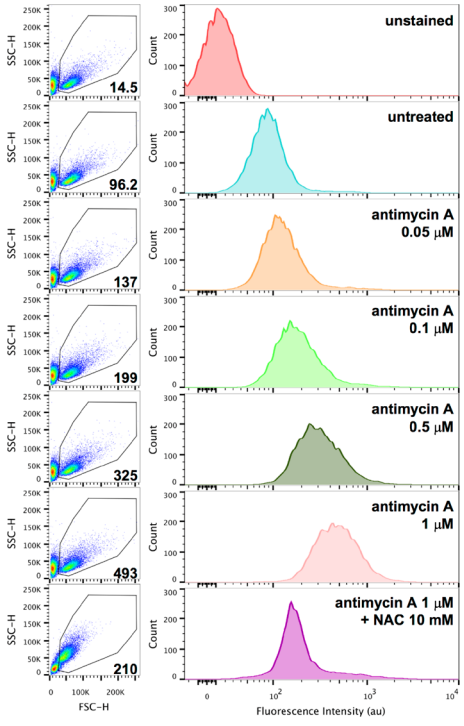

Figure 5. Quantitative application of **HKSOX-1r** in flow cytometry (FACS) analysis. RAW264.7 cells were coincubated with **HKSOX-1r** (4 μM), antimycin A (50, 100, 500, or 1000 nM) in the presence or absence of the antioxidant NAC (10 mM) for 30 min. Results are representative of at least three independent experiments. Representative dot plots (left) and histograms (right) of RAW264.7 cell response, as reported by **HKSOX-1r**. The unstained group (cells only) and untreated group (cells with 4 μM probe alone, 30 min) were included as controls.

(Figure S12), which suggested that theses probes are virtually nontoxic to cells when used at up to 10 μM after 24 h incubation.

To explore the potential of **HKSOX-1r** as an in vivo imaging tool, we applied it to $O_2^{\bullet-}$ detection in live zebrafish embryos (Figures 7 and S13). Briefly, 72 hpf (hours postfertilization) zebrafish embryos were anaesthetized (50 mg/L tricaine) and immersed in E3 buffer with **HKSOX-1r** (10 μM) for probe

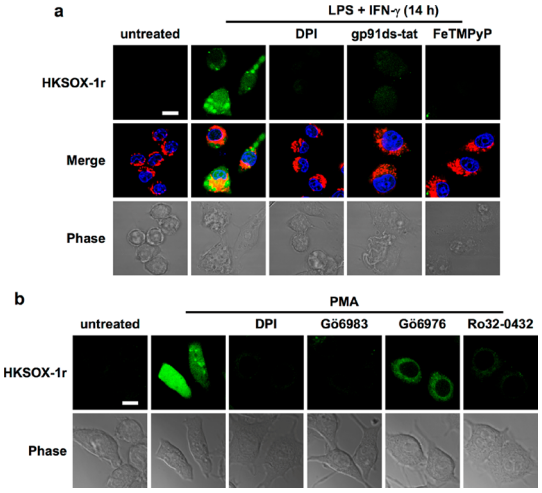

Figure 6. HKSOX-1r selectively detects $O_2^{\bullet-}$ under two types of immune stimulation. (a) Representative images of RAW264.7 mouse macrophages stimulated with LPS (500 ng/mL) and IFN-γ (50 ng/mL) for 14 h, in the absence or presence of DPI (50 nM), gp91ds-tat (2 μM), or FeTMPyP (50 μM). Cells were costained with mitochondrial dye MitoTracker Red (50 nM), nuclear DNA dye Hoechst 33342 (150 ng/mL), and **HKSOX-1r** (2 μM) for 30 min before confocal imaging. Merged: all fluorescence images merged. (b) Representative confocal images of RAW264.7 cells preloaded with **HKSOX-1r** (2 μM) for 30 min, and briefly challenged with PMA (200 ng/mL) in the absence or presence of DPI (50 nM) or a PKC inhibitor (Gö6983, Gö6976, or Ro32-0432; 100 nM). Scale bar = 10 μm.

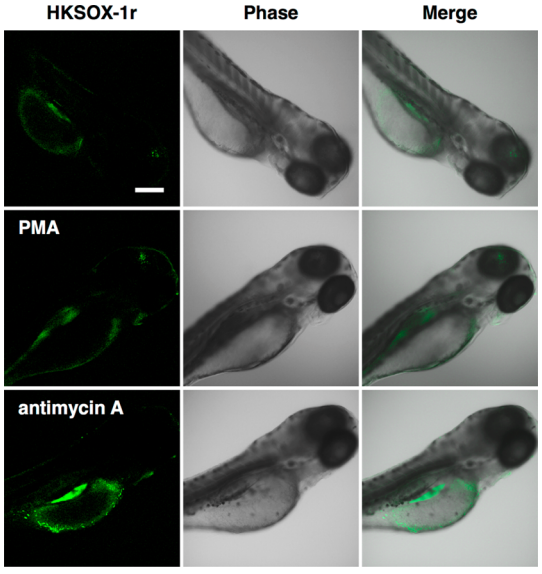

Figure 7. Confocal imaging of endogenous $O_2^{\bullet-}$ in 72 h postfertilization (hpf) zebrafish embryos. At 72 hpf, zebrafish embryos were first preloaded with **HKSOX-1r** (10 μM) for 20 min, and briefly challenged with PMA (200 ng/mL) or antimycin A (500 nM) for 15 min, before confocal imaging (at 10× magnification). Representative confocal images are shown. Merge: fluorescence and phase images merged. Scale bar = 200 μm.

loading. Embryos were then subjected to challenge of PMA or antimycin A. Compared to the untreated control, significantly increased $O_2^{\bullet-}$ levels were observed in PMA- or antimycin A-treated zebrafish, with distinct fluorescence distribution (Figure

DOI: 10.1021/jacs.5b01881
J. Am. Chem. Soc. 2015, 137, 6837−6843

7). These results suggest that **HKSOX-1r** penetrates tissues efficiently, and has potential utility in detecting $O_2^{\bullet-}$ in vivo.

CONCLUSION

Massive efforts have been invested on the development of fluorescent probes for ROS sensing, which are only matched by an ever expanding appetite for better tools to tackle controversies in ROS metabolism, dynamics, and functions. Yet for decades, accurate $O_2^{\bullet-}$ detection has remained a tantalizing goal due in part to the molecule's Janus-faced nature as an oxidant and reductant. In this work, we have discovered that $O_2^{\bullet-}$ can trigger aryl triflate cleavage efficiently and successfully applied this strategy to develop three novel $O_2^{\bullet-}$-selective fluorescent probes (**HKSOX-1/1r/1m**) for specific $O_2^{\bullet-}$ detection in the presence of excessive strong ROS and ubiquitous thiols found in live cells. The utility of **HKSOX-1/1r/1m** for $O_2^{\bullet-}$ imaging and detection has been fully demonstrated in terms of their outstanding sensitivity and selectivity. In particular, the probe **HKSOX-1r** gave a strong turn-on response toward $O_2^{\bullet-}$ in live cells and in vivo, and can be robustly applied to confocal imaging, 96-well microplate assay and flow cytometry analysis. We anticipate that further application of these probes will stimulate biomedical discoveries on the roles of $O_2^{\bullet-}$ in health and disease.

ASSOCIATED CONTENT

Supporting Information

Experimental details for chemical synthesis of all compounds, supplementary photophysical characterization of all probes, and imaging methods and data. The Supporting Information is available free of charge on the ACS Publications website at DOI: 10.1021/jacs.5b01881.

Web-Enhanced Features

Videos in avi format are available in the online version of this paper, showing the time-lapse confocal imaging of mitochondrial $O_2^{\bullet-}$ in differentiated human THP-1 macrophages under resting condition and antimycin A (1 μM; 30 min) stimulation, as visualized with **HKSOX-1m** (10 μM) over a period of 2 min (5 s per frame).

AUTHOR INFORMATION

Corresponding Author

*yangdan@hku.hk

Author Contributions

‖J.J.H. and N.-K.W. contributed equally.

Notes

The authors declare the following competing financial interest(s): D.Y., J.J.H. and N.K.W. hold patents on HKSOX-1, HKSOX-1r and HKSOX-1m.

ACKNOWLEDGMENTS

This work was supported by The University of Hong Kong, the University Development Fund, and Hong Kong Research Grants Council under General Research Fund Scheme (HKU 17305714). We thank Prof. Heping Cheng for expert advice, Dr. Derek Hoi-Hang Ho, Dr. Richard Yi-Tsun Kao, Dr. Yan Chen, Dr. Jing Guo, and Dr. Peng Gao for technical assistance, and the HKU Li Ka Shing Faculty of Medicine Faculty Core Facility and Zebrafish Core Facility, and the HKU School of Biological Sciences Central Facilities Laboratory for support in confocal microscopy. A.Y.-H.L. is the Li Shu Fan Medical Foundation Professor in Haematology and received funding from its endowment.

REFERENCES

(1) Winterbourn, C. C. *Nat. Chem. Biol.* **2008**, *4*, 278−286.
(2) Nathan, C.; Cunningham-Bussel, A. *Nat. Rev. Immunol.* **2013**, *13*, 349−361.
(3) Brownlee, M. *Nature* **2001**, *414*, 813−820.
(4) Halliwell, B.; Gutteridge, J. M. C. *Free Radicals in Biology and Medicine*; Oxford University Press: Oxford, 2007, 1−677.
(5) Imlay, J. A. *Annu. Rev. Biochem.* **2008**, *77*, 755−776.
(6) Imlay, J. A. *Nat. Rev. Microbiol.* **2013**, *11*, 443−454.
(7) Winterbourn, C. C.; Metodiewa, D. *Free Radical Biol. Med.* **1999**, *27*, 322−328.
(8) Dixon, S. J.; Stockwell, B. R. *Nat. Chem. Biol.* **2014**, *10*, 9−17.
(9) Archer, S. L. *N. Engl. J. Med.* **2013**, *369*, 2236−2251.
(10) Cai, H.; Harrison, D. G. *Circ. Res.* **2000**, *87*, 840−844.
(11) Rose, S.; Melnyk, S.; Pavliv, O.; Bai, S.; Nick, T. G.; Frye, R. E.; James, S. J. *Transl. Psychiatry* **2012**, *2*, e134.
(12) Mattson, M. P. *Nature* **2004**, *430*, 631−639.
(13) Cairns, R. A.; Harris, I. S.; Mak, T. W. *Nat. Rev. Cancer* **2011**, *11*, 85−95.
(14) Gorrini, C.; Harris, I. S.; Mak, T. W. *Nat. Rev. Drug Discovery* **2013**, *12*, 931−947.
(15) Murphy, M. P.; Holmgren, A.; Larsson, N.-G.; Halliwell, B.; Chang, C. J.; Kalyanaraman, B.; Rhee, S. G.; Thornalley, P. J.; Partridge, L.; Gems, D.; Nyström, T.; Belousov, V.; Schumacker, P. T.; Winterbourn, C. C. *Cell Metab.* **2011**, *13*, 361−366.
(16) Wei, L.; Dirksen, R. T. *J. Gen. Physiol.* **2012**, *139*, 425−434.
(17) Fang, F. C. *Nat. Biotechnol.* **2013**, *31*, 415−416.
(18) Wardman, P. *Free Radical Biol. Med.* **2007**, *43*, 995−1022.
(19) Li, X.; Gao, X.; Shi, W.; Ma, H. *Chem. Rev.* **2013**, *114*, 590−659.
(20) Robinson, K. M.; Janes, M. S.; Pehar, M.; Monette, J. S.; Ross, M. F.; Hagen, T. M.; Murphy, M. P.; Beckman, J. S. *Proc. Natl. Acad. Sci. U.S.A.* **2006**, *103*, 15038−15043.
(21) Zielonka, J.; Kalyanaraman, B. *Free Radical Biol. Med.* **2010**, *48*, 983−1001.
(22) Tarpey, M. M.; Fridovich, I. *Circ. Res.* **2001**, *89*, 224−236.
(23) Kundu, K.; Knight, S. F.; Willett, N.; Lee, S.; Taylor, W. R.; Murthy, N. *Angew. Chem., Int. Ed.* **2009**, *48*, 299−303.
(24) Zhang, W.; Li, P.; Yang, F.; Hu, X.; Sun, C.; Zhang, W.; Chen, D.; Tang, B. *J. Am. Chem. Soc.* **2013**, *135*, 14956−14959.
(25) Maeda, H.; Yamamoto, K.; Nomura, Y.; Kohno, I.; Hafsi, L.; Ueda, N.; Yoshida, S.; Fukuda, M.; Fukuyasu, Y.; Yamauchi, Y.; Itoh, N. *J. Am. Chem. Soc.* **2005**, *127*, 68−69.
(26) Maeda, H.; Yamamoto, K.; Kohno, I.; Hafsi, L.; Itoh, N.; Nakagawa, S.; Kanagawa, N.; Suzuki, K.; Uno, T. *Chem.—Eur. J.* **2007**, *13*, 1946−1954.
(27) Xu, K. H.; Liu, X.; Tang, B.; Yang, G. W.; Yang, Y.; An, L. G. *Chem.—Eur. J.* **2007**, *13*, 1411−1416.
(28) Murale, D. P.; Kim, H.; Choi, W. S.; Churchill, D. G. *Org. Lett.* **2013**, *15*, 3946−3949.
(29) Sun, W.-C.; Gee, K. R.; Klaubert, D. H.; Haugland, R. P. *J. Org. Chem.* **1997**, *62*, 6469−6475.
(30) Izumi, S.; Urano, Y.; Hanaoka, K.; Terai, T.; Nagano, T. *J. Am. Chem. Soc.* **2009**, *131*, 10189−10200.
(31) Zhao, H.; Kalivendi, S.; Zhang, H.; Joseph, J.; Nithipatikom, K.; Vasquez-Vivar, J.; Kalyanaraman, B. *Free Radical Biol. Med.* **2003**, *34*, 1359−1368.
(32) Sawyer, D. T.; Valentine, J. S. *Acc. Chem. Res.* **1981**, *14*, 393−400.
(33) West, A. P.; Shadel, G. S.; Ghosh, S. *Nat. Rev. Immunol.* **2011**, *11*, 389−402.
(34) Sahin, E.; DePinho, R. A. *Nat. Rev. Mol. Cell Biol.* **2012**, *13*, 397−404.
(35) Zhou, R.; Yazdi, A. S.; Menu, P.; Tschopp, J. *Nature* **2011**, *469*, 221−225.

DOI: 10.1021/jacs.5b01881
J. Am. Chem. Soc. 2015, 137, 6837−6843

(36) (a) Lambert, A. J.; Brand, M. D. *Methods Mol. Biol.* **2009**, *554*, 165−181. (b) Kuznetsov, A. V.; Veksler, V.; Gellerich, F. N.; Saks, V.; Margreiter, R.; Kunz, W. S. *Nat. Protoc.* **2008**, *3*, 965−976.
(37) Bedard, K.; Krause, K.-H. *Physiol. Rev.* **2007**, *87*, 245−313.
(38) Lambeth, J. D. *Nat. Rev. Immunol.* **2004**, *4*, 181−189.
(39) West, A. P.; Brodsky, I. E.; Rahner, C.; Woo, D. K.; Erdjument-Bromage, H.; Tempst, P.; Walsh, M. C.; Choi, Y.; Shadel, G. S.; Ghosh, S. *Nature* **2011**, *472*, 476−480.
(40) Peng, T.; Wong, N.-K.; Chen, X.; Chan, Y.-K.; Ho, D. H.-H.; Sun, Z.; Hu, J. J.; Shen, J.; El-Nezami, H.; Yang, D. *J. Am. Chem. Soc.* **2014**, *136*, 11728−11734.
(41) Zipfel, M.; Carmine, T. C.; Gerber, C.; Niethammer, D.; Bruchelt, G. *Biochem. Biophys. Res. Commun.* **1997**, *232*, 209−212.
(42) Kagan, V. E.; Konduru, N. V.; Feng, W.; Allen, B. L.; Conroy, J.; Volkov, Y.; Vlasova, I. I.; Belikova, N. A.; Yanamala, N.; Kapralov, A.; Tyurina, Y. Y.; Shi, J.; Kisin, E. R.; Murray, A. R.; Franks, J.; Stolz, D.; Gou, P.; Klein-Seetharaman, J.; Fadeel, B.; Star, A.; Shvedova, A. A. *Nat. Nanotechnol.* **2010**, *5*, 354−359.
(43) Sergeant, S.; McPhail, L. C. *J. Immunol.* **1997**, *159*, 2877−2885.
(44) Pongracz, J.; Lord, J. M. *Biochem. Biophys. Res. Commun.* **1998**, *247*, 624−629.

DOI: 10.1021/jacs.5b01881
J. Am. Chem. Soc. 2015, 137, 6837−6843